CHALMERS
UNIVERSITY OF TECHNOLOGY

Contactless Measurement of a D-Band On-Chip Antenna Using an Integrated Reflective Load Switch

Contactless Measurement of a D-Band On-Chip Antenna Using an Integrated Reflective Load Switch

Dmitrii Kruglov, *Student Member, IEEE,* Pavlo Krasov, *Member, IEEE,* Oleg Iupikov, *Member, IEEE,* Artem Vilenskiy, *Member, IEEE,* Marianna Ivashina, *Senior Member, IEEE,* and Rob Maaskant, *Senior Member, IEEE*

***Abstract*—A novel measurement setup is proposed for the contactless characterization of on-chip antennas. A D-band patch antenna is fabricated on a 100 µm-thick GaAs substrate and is monolithically integrated with a reflective load switch to allow for fast electronic control of the antenna port termination. The antenna under test is illuminated by a reference antenna in the anechoic chamber after which the impedance and gain of the patch antenna are reconstructed from the change in backscattered field due to different port terminations. In our experiment, the over-the-air reconstructed antenna input impedance exhibits a frequency shift of less than 1% with respect to the (non-ideal) on-wafer probe measurement in the 115–130 GHz frequency range. Furthermore, the measured realized gain of 0.9 ± 0.5 dBi is close to the simulated one of 1.1 dBi.**

I. Introduction

Many wireless applications require antennas to be tightly integrated with analogue electronics. Consequently, the antenna port may no longer be physically accessible, which complicates the antenna characterization [1]. Moreover, re-routing the antenna signal to an external connector without introducing additional uncertainties is challenging, particularly at mm-wave frequencies, and may not be calibrated out with high precision. In addition, measuring an on-wafer antenna using a ground-signal-ground (GSG) probe is a major challenge because the probe may affect the field that is emitted by the antenna, further obscuring the measurement results [2].

One of the probeless measurement procedures that overcomes the above challenges utilizes the so-called backscattering modulation method [3]. In this method a reference antenna (RA) illuminates an antenna under test (AUT) inside an anechoic chamber which then scatters and re-radiates a field depending upon the AUT load termination. The change in the re-radiated portion of the field modulates the S_{11} of the reference antenna, which allows us to reconstruct the gain and impedance of the AUT [3]. This type of over-the-air characterization has also been used to reconstruct the port-to-port coupling in multi-port AUTs [4].

The backscattering modulation method has been practically demonstrated for AUT impedance reconstruction below 1 GHz, where the load-switching board was externally connected to the AUT, i.e., via a standard SMA connector interface [5]. A practical application of this technique is e.g. cell phone antenna measurement in real-life radiation conditions [6]. Recently, the method has been extended with an accurate gain estimation technique and been practically demonstrated up to 40 GHz for an open-ended waveguide AUT utilizing a 2.92 mm coaxial interface [7]. It has to be noted that the disturbances in the measurement setup introduced during manual load switching can lead to significant errors [8], which emphasizes the necessity to modulate the antenna load impedance electronically, especially at high frequencies. This promising method has yet to be demonstrated at higher frequencies and/or for highly integrated antennas where no coaxial or waveguide interfaces exists.

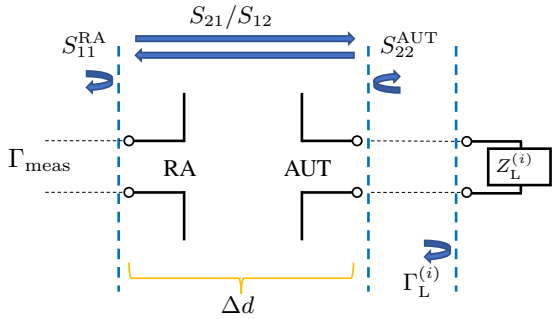

Fig. 1: The OTA measurement setup. The reference antenna (RA) is connected to the VNA, the antenna under test (AUT) is connected to an electronically-controlled load $Z_L^{(i)}$. The separation Δd is varied in the experiment.

To the author's best knowledge, the backscattering modulation method has not yet been applied to integrated on-chip or in-package antennas. Novel contributions of this work are:

- Demonstration of the contactless OTA antenna characterization method above 100 GHz for on-chip antennas
- Integration of on-chip antenna with electronic load-switch to enable the OTA measurement

In Sec. II a summary of the contactless antenna characterization method is provided, after which the specific architecture of our prototype is presented in Sec. III. Finally, the results are discussed in Sec. IV and conclusions are drawn in Sec. V.

II. Method Description

Fig. 1 shows a 2-port network model of the OTA setup. By terminating the AUT by $Z_L^{(i)}$ (providing the reflection

This work has received funding from the European Union's Horizon 2020 research and innovation programme under the Marie Skłodowska-Curie grant agreements No 860023 and PENTA-EURIPIDES InnoStar project (No. 2021-04055).

The authors are with the Chalmers University of Technology, Department of Electrical Engineering, S-41296 Gothenburg, Sweden. (e-mail: dmitrii.kruglov@chalmers.se)

coefficient $\Gamma_{\rm L}^{(i)}$), the total reflection $\Gamma_{\rm meas}^{(i)}$ that is measured at the RA antenna port is found to be

$$\Gamma_{\rm meas}^{(i)} = S_{11}^{\rm RA} + \frac{S_{12}S_{21}\Gamma_{\rm L}^{(i)}}{1 - S_{22}^{\rm AUT}\Gamma_{\rm L}^{(i)}} \tag{1}$$

which is a well-known result put-to-use in 1-port calibrations. Eq. (1) can be rewritten as

$$\Gamma_{\rm meas}^{(i)} = S_{11}^{\rm RA} + S_{22}^{\rm AUT}\Gamma_{\rm meas}^{(i)}\Gamma_{\rm L}^{(i)} + (S_{21}^2 - S_{11}^{\rm RA}S_{22}^{\rm AUT})\Gamma_{\rm L}^{(i)} \tag{2}$$

where a reciprocal system is assumed (i.e. $S_{21} = S_{12}$). For measurements $i = 1, \ldots, N$ this leads to the matrix equation

$$\begin{bmatrix} \Gamma_{\rm meas}^{(1)} \\ \Gamma_{\rm meas}^{(2)} \\ \vdots \\ \Gamma_{\rm meas}^{(N)} \end{bmatrix} = \begin{bmatrix} 1 & \Gamma_{\rm meas}^{(1)}\Gamma_{\rm L}^{(1)} & \Gamma_{\rm L}^{(1)} \\ 1 & \Gamma_{\rm meas}^{(2)}\Gamma_{\rm L}^{(2)} & \Gamma_{\rm L}^{(2)} \\ \vdots & \vdots & \vdots \\ 1 & \Gamma_{\rm meas}^{(N)}\Gamma_{\rm L}^{(N)} & \Gamma_{\rm L}^{(N)} \end{bmatrix} \begin{bmatrix} S_{11}^{\rm RA} \\ S_{22}^{\rm AUT} \\ S_{21}^2 - S_{11}^{\rm RA}S_{22}^{\rm AUT} \end{bmatrix} \tag{3}$$

which can be solved if $N \geq 3$, i.e., if one uses at least three different loads $Z_{\rm L}^{(i)}$.

The AUT impedance is readily available from $S_{22}^{\rm AUT}$. Furthermore, Friis equation states that S_{21}^2 is related to the farfield gain product $G^{\rm RA}G^{\rm DUT}$ of the RA and AUT, i.e.,

$$G^{\rm RA}G^{\rm AUT} = |S_{21}|^2 \left(\frac{4\pi(\Delta d - \hat{d}_0)}{\lambda_0}\right)^2, \tag{4}$$

where Δd is the physical separation between the two antennas, which is a parameter that we control in the experiment, and $\hat{d}_0$ is the offset between Δd and the "true" phase center-to-center distance $d' = (\Delta d - \hat{d}_0)$. The gain product must be independent on Δd in the far field, so we follow the procedure outlined in [7] to find $\hat{d}_0$ that accomplishes this goal. After finding d', the AUT gain follows from

$$G^{\rm AUT} = |S_{21}|^2 \left(\frac{4\pi d'}{\lambda_0}\right)^2 / G^{\rm RA} \tag{5}$$

where we assume the gain of the reference antenna to be known.

III. Device Architecture

To characterize the antenna of a highly-integrated wireless integrated circuit (IC) [Fig. 2(a)], we propose a test device with the same chip area as the live design, but with an electronically-controlled load switch replacing the analogue circuitry [Fig. 2(b)]. This way, the antenna can be characterized in the same radiation conditions as in the live design using the backscattering modulation method. We also fabricated an antenna with GSG RF probe pads [Fig. 2(c)] to compare the OTA and the on-wafer measurements.

Our test devices are realized in the commercial PIN-pHEMT GaAs process PIH1-10 from WIN Semiconductors. The process offers two gold layers in the back-end-of-line separated by silicon nitride (SiN) and polyimide (PI) layers on a 100 μm GaAs substrate.

A. Load Switch IC Design

Based on Eq. (1), in the extreme cases of a perfectly matched or completely mismatched AUT

$$\Gamma_{\rm meas}^{(j)} - \Gamma_{\rm meas}^{(i)} \propto \begin{cases} \Gamma_L^{(j)} - \Gamma_L^{(i)} & , \text{if } S_{22}^{\rm AUT} = 0 \\ \frac{\Gamma_L^{(j)} - \Gamma_L^{(i)}}{(1-\Gamma_L^{(j)})(1-\Gamma_L^{(i)})} & , \text{if } S_{22}^{\rm AUT} = 1 \end{cases} \tag{6}$$

We observe that the dynamic range of the measurement setup strongly depends on $\Gamma_L^{(i)}$, and is the largest when the distance between $\Gamma_L^{(i)}$ in the complex plane is the largest (e.g. $||\Gamma_L^{(i)}|| = 1$ with 120° phase difference in a 3-loads case) — which is what we aimed for in our design.

Fig. 3 shows the load switch schematics, which consists of two in-series *p-i-n* diodes $\mathbf{D_1}$ and $\mathbf{D_2}$ with a decoupling capacitor $\mathbf{C_d}$ (0.25 pF) to separate their DC currents. We used tuning short and open transmission line stubs $\mathbf{TL_{m,1}}$ ($50\Omega\angle 48°$) and $\mathbf{TL_{m,2}}$ ($41.5\Omega\angle 43°$) to achieve desirable $\Gamma_L^{(i)}$ responses. The DC biasing lines $\mathbf{TL_b}$ ($65.7\Omega\angle 47°$) and decoupling capacitors $\mathbf{C_b}$ (1.2 pF) are shown in blue. The microphotograph of the fabricated device is also presented in Fig. 3.

B. On-chip Patch Antenna Design

Fig. 4 shows the HFSS model of the standalone on-chip cavity-backed patch antenna. The top metal layer (M2) accommodates a radiating patch, while a microstrip line in the lower layer (M1) forms the proximity-coupled feed. Patch cavity walls are formed by thru-substrate vias. Ansys HFSS finite element solver was used to optimize antenna impedance matching at 120 GHz on an infinitely large ground plane. The width of the radiating patch is $w_1 = 490$ µm, length is $l_1 = 325$ µm, the coupling patch is a square with a side of $w_2 = 80$ µm and is offset by $y_f = 110$ µm from the radiating patch center.

Fig. 5 shows two antenna designs: one integrated directly with the load switch, and the other interfaced with ground-signal-ground pads for on-wafer probing. These correspond to Fig. 2(b) and Fig. 2(c) respectively. The design on the left was diced from the wafer, glued to the PCB (Fig. 7), and used in the OTA measurement. This allows us to compare the OTA measurement with the on-wafer measurement.

IV. Measurement Results

A. On-Wafer Measurements

Fig. 6 displays the on-wafer measured $\Gamma_L^{(i)}$ of the load switch in Fig. 3. All on-wafer measurements reported here

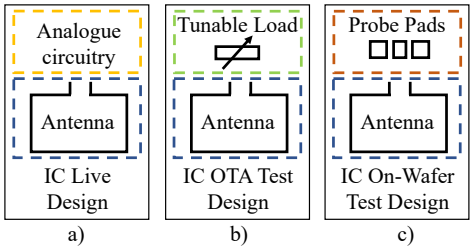

Fig. 2: (a) Intended "live" IC design; (b)-(c) considered test chips for the antenna characterization.

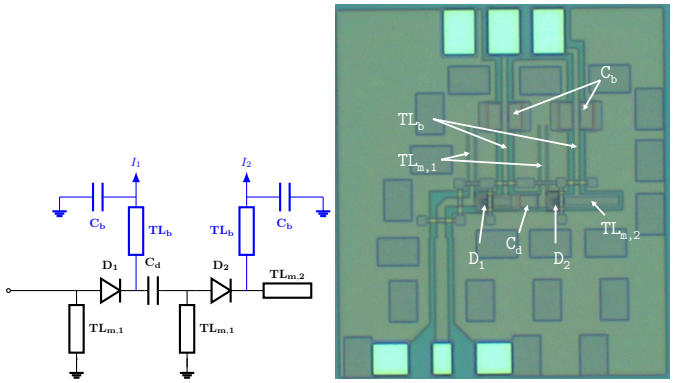

Fig. 3: Schematics of the reflective load switch (left) and the photograph of the 1×0.59 mm^2 fabricated device (right).

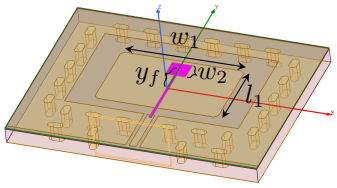

Fig. 4: HFSS model of the antenna. The pink highlighted proximity-coupled feeding line.

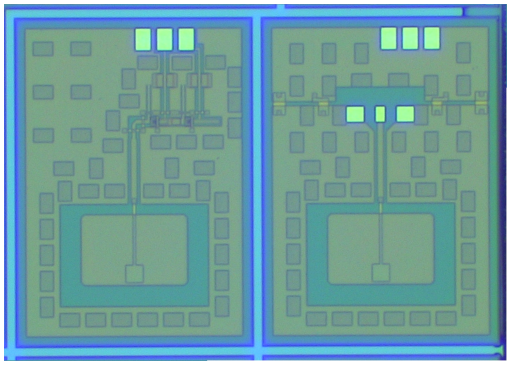

Fig. 5: A photograph of the antenna integrated with a load switch made for OTA measurement (left), and the standalone antenna made for on-wafer characterization (right). The area of a single fabricated device is 1.42×1 mm^2

are shown after the probe pads and input feed lines have been calibrated out using thru-reflect-line (TRL) calibration procedure. We denote the closed (no DC current) state of the diode as '0' and the open state as '1'. The load switch state is described by two numbers $[ij]$, where i and j are either '0' or '1' depending on whether the first and second diodes are closed or open. Due to the diode's parasitic losses in all states, the switch response curves do not reach the edge of the Smith chart. The load switch responses shown in Fig. 6 are the $\Gamma_L^{(i)}$ values we used to reconstruct the parameters of the AUT.

B. Contactless OTA Antenna Measurement

The contactless OTA measurements were performed in the Chalmers THz anechoic chamber (AC). Fig. 7 shows how the chip is glued onto a base PCB. The chip's DC pads controlling the diodes' current are connected via bond wires to this PCB, which are then connected to the DC current source. The AUT is then fixed to one side of the AC, while the RA is mounted on a movable stand opposite and collinear to the AUT (Fig. 8).

Due to large free-space path loss, it is crucial to keep the RA-to-AUT separation distance small enough to minimize signal loss and large enough to meet the farfield conditions. Fig. 9 shows the gain product $G^{\mathrm{RA}}G^{\mathrm{AUT}}$ at 120 GHz vs Δd distance sweep (step size is 0.02 cm), where Δd is the distance between the apertures of the antennas. For each Δd we measure $\Gamma_{\mathrm{meas}}^{(i)}$ for each $\Gamma_{\mathrm{L}}^{(i)}$, shown in Fig. 6, three times, for averaging purposes. The so-estimated $\Gamma_{\mathrm{meas}}^{(i)}$ and $\Gamma_{\mathrm{L}}^{(i)}$ are then used to solve Eq. (3) to extract S_{21}. Eq. (4) is then plotted for various $\hat{d}_0$. We observe that $\hat{d}_0 = -2$ cm yields the most constant pair gain, which allows us to estimate the actual phase center-to-center distance between the antennas (top axis) [7].

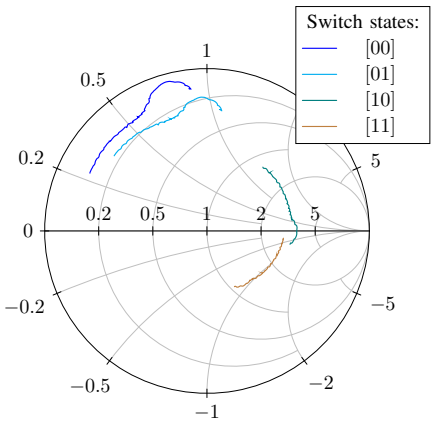

Fig. 6: Measurements of the load switch from Fig. 3 in the 115 to 130 GHz frequency range. $I_{\mathrm{on}} = 10$ mA, $I_{\mathrm{off}} = 0$ mA.

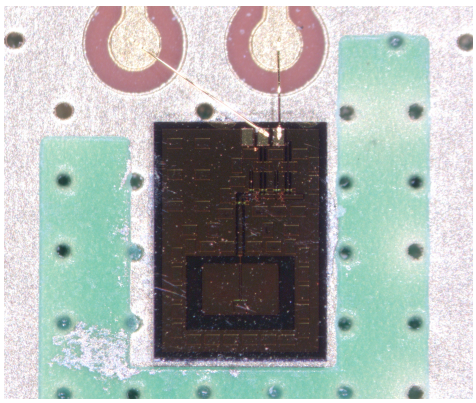

Fig. 7: Test device mounted on the PCB.

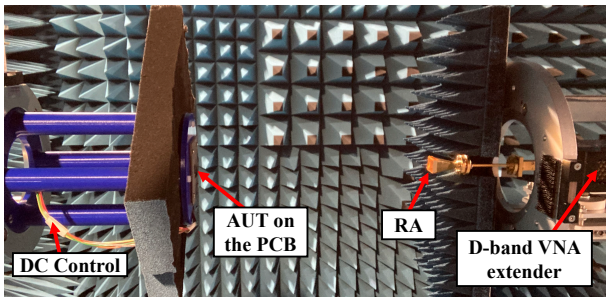

Fig. 8: Anechoic chamber setup.

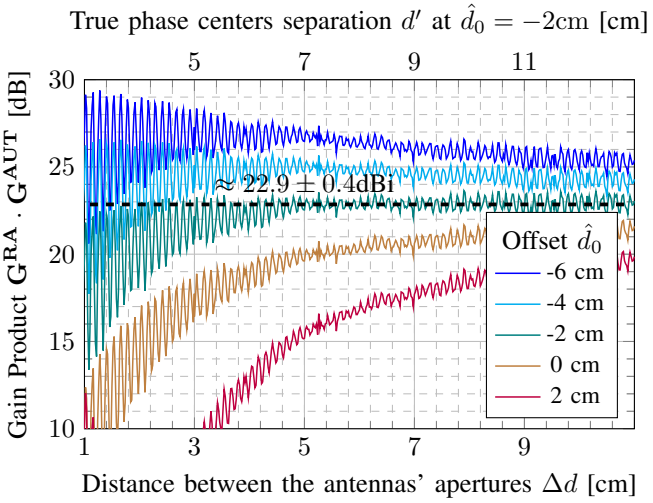

Fig. 9: Gain product based on eq. 4 used to determine an accurate phase-to-phase distance and the gain of the AUT at 120 GHz from the OTA measurements. Top axis shows the calculated true distance between antenna phase centers.

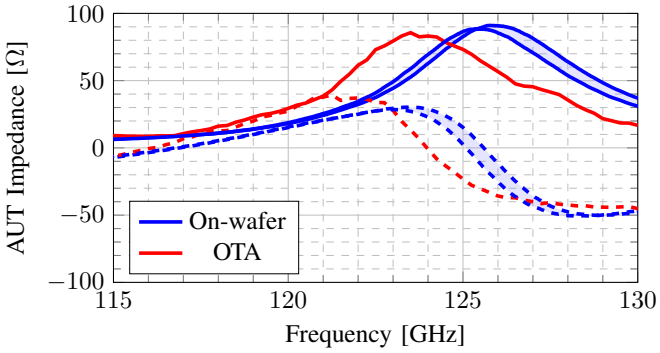

Fig. 10: OTA antenna impedance reconstruction vs on-wafer measurements. The real part is shown in solid lines, and the imaginary - in dashes. The on-wafer measurement was repeated on three different locations on the wafer, the range of values is shown as filled area between the extremes.

It corresponds to the pair gain product of 22.9 dBi with a ± 0.4 dBi ripple. The gain of the RA is 22 ± 0.3 dBi. Thus, the (realized) DUT gain at 120 GHz is estimated to be 0.9 ± 0.5 dBi in the broadside. HFSS-simulated gain of the antenna assuming infinite perfect ground plane is 1.1 dBi.

Based on Fig. 9, we choose $\Delta d = 5$ cm as the operation point for our measurements because it is the shortest distance at which the farfield conditions are satisfied. This corresponds to $d' = 7$ cm phase center-to-center separation, for which the free-space path loss between the antennas according to the Friis equation is -50 dB at 120 GHz, or -100 dB two-ways. The loss in the load switch, taking the worst case in the 115–130 GHz range from the measurements in Fig. 6, adds up to 5 dB more loss. Counting in the pair gain of 22.9 dBi from fig. 9, we see that the strength of the captured signal re-radiated from the AUT is ≈ -80 dB. This becomes comparable to the VNA receiver drift which we estimate to be of the order of -90 dB over 1 minute, and thus one has to measure $\Gamma^{(i)}_{\text{meas}}$ for consecutive $\Gamma^{(i)}_{\text{L}}$ before the drift error becomes comparable to the magnitudes of $\Gamma^{(i)}_{\text{meas}}$. Since we perform automated measurements through a MATLAB© script, three measurements of $\Gamma^{(i)}_{\text{meas}}$ for four $\Gamma^{(i)}_{\text{L}}$ values per Δd and per frequency point takes $\sim$10 sec. This way, drifts are well below -95 dB, giving us $10-15$ dB of dynamic range. Furthermore, we prevented the PiN diodes from overheating by leaving them in the [0,0]-state between the $\Gamma^{(i)}_{\text{L}}$ settings so that the on-wafer load switch calibration table remains accurate. The OTA measurements were taken in the $110 - 130$ GHz frequency range (0.25 GHz step), and to reduce the standing wave effect between the probe and AUT, we averaged the measurements over the $5.00-5.24$ cm Δd-range with 0.02 cm step size.

The result of the AUT impedance reconstruction is compared to the on-wafer antenna measurement in Fig. 10, simulation results are omitted to focus on this comparison. The 1 GHz offset in resonant frequency and the 10 Ω difference in the real component of the antenna input impedance can be attributed to the influence of the RF probe and variations in environment's conditions: one measurement involved the antenna being evaluated on-wafer within a high-permittivity dielectric environment, while in the other the antenna was mounted on the top of the PCB's ground plane. Deviation from the simulated result of 120 GHz can be attributed to process variations in substrate thickness and permittivity.

V. Conclusion

Measuring millimeter-wave antennas presents significant challenges, particularly when integrated closely with on-chip or in-package electronics. If the antenna lacks an easily-accessible RF interface, such as waveguide or coaxial connector, it has to be measured with RF probes that ultimately interfere with the antenna radiation. Contactless over-the-air characterization technique can address this concern by eliminating the reliance on probes and enabling fabrication and assembly of the test device in close-to-real-world usage conditions. However, it introduces its own complications, as free-space path loss increases rapidly with greater antenna separation, while a meaningful result can only be achieved if it is greater than the far-field distance. In our study, we combined a novel approach of using electronically controlled load switch for real-time measurement with the method from [7] that allows using optimal antenna separation, maximizing the dynamic range of the measurement setup. We propose this technique for scenarios demanding accurate antenna characterization in realistic radiation condition, and the probe-based method for rapid verification.

Acknowledgment

The authors would like to thank WIN Semiconductors Corporation for fabricating the circuits as a part of WIN's university multi-project wafer program. Authors also express gratitude to Vessen Vassilev from Chalmers University MC2 department and Markus Gavell from Gotmic A.B. for helping with the on-wafer measurements, and to Ulf Johannsen and Sander Bronckers from the Eindhoven University of Technology (TU/e) for sharing their practical experience on the contactless backscattering method.

REFERENCES

[1] Y. Zhang and J. Mao, "An overview of the development of antenna-in-package technology for highly integrated wireless devices," *Proceedings of the IEEE*, vol. 107, no. 11, pp. 2265–2280, 2019.

[2] A. C. F. Reniers, A. R. van Dommele, A. B. Smolders, and M. H. A. J. Herben, "The influence of the probe connection on mm-wave antenna measurements," *IEEE Transactions on Antennas and Propagation*, vol. 63, no. 9, pp. 3819–3825, 2015.

[3] W. Wiesbeck and E. Heidrich, "Wide-band multiport antenna characterization by polarimetric rcs measurements," *IEEE Transactions on Antennas and Propagation*, vol. 46, no. 3, pp. 341–350, 1998.

[4] B. Monsalve, S. Blanch, and J. Romeu, "Multiport small integrated antenna impedance matrix measurement by backscattering modulation," *IEEE transactions on antennas and propagation*, vol. 61, no. 4, pp. 2034–2042, 2013.

[5] B. Monsalve, S. Blanch, J. Romeu, and L. Jofre, "A contact-less small antenna characterization through impedance modulation," in *2009 3rd European Conference on Antennas and Propagation*. IEEE, 2009, pp. 696–698.

[6] B. Monsalve, S. Blanch, and J. Romeu, "Input impedance measurements of cell phone antennas using backscattering modulation," in *2012 6th European Conference on Antennas and Propagation (EUCAP)*. IEEE, 2012, pp. 1549–1551.

[7] A. Van Den Biggelaar, S. J. Geluk, B. F. Jamroz, D. Williams, A. Smolders, U. Johannsen, and L. A. Bronckers, "Accurate gain measurement technique for limited antenna separations," *IEEE Transactions on Antennas and Propagation*, vol. 69, no. 10, pp. 6772–6782, 2021.

[8] A. van den Biggelaar, D. Daverveld, A. C. Reniers, U. Johannsen, and A. Smolders, "Assessment of a contactless characterization method for integrated antennas," in *2019 16th European Radar Conference (EuRAD)*. IEEE, 2019, pp. 381–384.